How Epithelial Cells Reorient in Response to Cyclic Stretching

Jui-Chien Lien
Carnegie Mellon University
Yu-Li Wang (yuliwang@andrew.cmu.edu)
Carnegie Mellon University

Research Article

Keywords: Epithelial, Cyclic Stretching, microtubule-modulated

Posted Date: March 24th, 2021

DOI: https://doi.org/10.21203/rs.3.rs-347408/v1

Version of Record: A version of this preprint was published at Scientific Reports on July 20th, 2021. See the published version at https://doi.org/10.1038/s41598-021-93987-y.

Main Manuscript for

How Epithelial Cells Reorient in Response to Cyclic Stretching

Jui-Chien Lien[a] and Yu-Li Wang[a,*]

[a]Department of Biomedical Engineering, Carnegie Mellon University, Pittsburgh, PA 15213

Corresponding author: Yu-Li Wang

Email: yuliwang@andrew.cmu.edu.

This file includes:

Main Text
Figures 1 to 7

Abstract

Many types of adherent cells are known to reorient upon uniaxial cyclic stretching perpendicularly to the direction of stretching to facilitate such important events as wound healing, angiogenesis, and morphogenesis. While this phenomenon has been documented for decades, the underlying mechanism remains poorly understood. Using an on-stage stretching device that allowed programmable stretching with synchronized imaging, we found that the reorientation of NRK epithelial cells took place primarily during the relaxation phase when cells underwent rapid global retraction followed by extension transverse to the direction of stretching. Inhibition of myosin II caused cells to orient along the direction of stretching, whereas disassembly of microtubules enhanced transverse reorientation. Our results indicate distinct roles of stretching and relaxation in cell reorientation and implicate a role of myosin II-dependent contraction via a microtubule-modulated mechanism. The importance of relaxation phase also explains the difference between the responses to cyclic and static stretching.

Introduction

Increasing attention has been paid over past decades to the effect of external mechanical signals, such as stretching forces and substrate stiffness, on cellular behavior, including growth, shape, adhesion, polarity, and migration[1-4]. In particular, cyclic stretching takes place ubiquitously in the body, driven for example by beating of the heart, inflation of the lungs, or peristalsis of the gut. Many types of cells, including smooth muscle cells, endothelial cells, and epithelial cells, are exposed to cyclic stretching to affect both physiological and pathological events. For instance, elevated cyclic stretching was proposed to induce aortic valve calcification[5], while proper stretching activities promote the differentiation of embryonic stem cells into muscle cells[6].

As was first discovered four decades ago, cyclic stretching caused fibroblasts to reorient perpendicularly to the direction of stretching[7]. Subsequent studies confirmed that many different types of adherent cells, such as endothelial and epithelial cells, can realign similarly when exposed to uniaxial cyclic stretching[8-12]. It is generally believed that this stretch-induced realignment is of importance to such events as wound healing, angiogenesis, and morphogenesis[13-16]. The intriguing response, accompanied by reorganization of actomyosin contractility and realignment of the actin and microtubule cytoskeleton[17-22], prompted various hypotheses based, for example, on the maintenance of tensional homeostasis or dissipation of stored elastic energy[9,23,24]. In addition to the contraction of actin cytoskeleton, microtubules may also play a regulatory role by stabilizing the cell shape and polarity[18,19,25].

Stretching-induced transverse reorientation is sensitive to the amplitude, frequency, and waveform of stretching[9,10]. The response requires a minimal strain of around 3%[26], above which the extent of reorientation shows a correlation with the magnitude of strain. Interestingly, static uniaxial stretching was found to cause cells to spread and migrate toward the direction of

46 stretching[27,28], in contrast to the transverse reorientation induced by cyclic stretching. Fibroblasts
47 reorientation requires a minimal frequency of 0.01 Hz and saturates at 1 Hz, while smooth muscle
48 cells show optimal realignment responses at 0.5 Hz[9,29]. Triangular, square, or asymmetric
49 waveforms induce different extents of cell reorientation and stress fiber redistribution[10,30], which
50 suggests sensitivities to the slopes of stretching and/or duration of stretching/relaxation.

51 The above observations suggest that, to unveil the mechanism of cyclic stretching-induced cell
52 orientation, it is important to understand potentially differential responses during the stretching
53 and relaxation phases. To this end, we have developed an on-stage cell stretcher based on a
54 motorized microscope stage and an elastic, patternable polyacrylamide substrate. The system
55 was programmed to allow synchronized image recording and cyclic stretching. Differences
56 between consecutive images then revealed changes in cell shape during different stages of cyclic
57 stretching and led us to a working model for transverse cell reorientation.

Results

Reorientation Response of NRK-52E Epithelial Cells to Cyclic Stretching

NRK-52E cells, a rat kidney epithelial cell line that exhibits high circularity and large spreading area at steady state, were used for studying shape responses to cyclic stretching. A novel stretcher for real-time imaging was developed using a microscope with a motorized stage. Cells were cultured on an elastic polyacrylamide (PAA) substrate 400 um in thickness. One end of the substrate was attached to the supporting coverslip underneath, which moved with the motorized stage. The other end was anchored with a rod, which pushed against a handle attached to the surface (Fig. 1a and 1b). A custom computer program allowed synchronized image acquisition at various times relative to the stretching cycle (Fig. 1a and 1b).

We used PAA gels with a Young's modulus of 20-30 kPa (prepared with 10% acrylamide and 0.3% bis-acrylamide), which is in the physiological range of tissue stiffness, as the substrate. Micropatterns on the gel surface was used to indicate the applied strain (Fig. 1c; Supplementary Fig. 1f, 1i, and 1k). The gel showed a nearly ideal elastic behavior when stretched by up to 20% at 0.5 Hz in a square waveform (Fig. 1d). Upon relaxation from 45 min of continuous cyclic stretching with 15% strain, the residual strain was <0.72% along the direction of stretching (referred to as axial) and <0.55% along a perpendicular direction (referred to as transverse) (Supplementary Fig. 2). The substrate remained intact following >72h of up to 18% of continuous cyclic stretching at 0.5Hz. In addition, transverse strain remained below 16% of axial strain, suggesting that the strain was predominantly uniaxial (Fig. 1d).

To avoid the complications of cell-cell mechanical interactions, we have limited the analysis to isolated cells. With 15% of cyclic strain at 0.4-0.5 Hz, cells started to show shape change as soon as 5 min and became oriented in a transverse direction within 30min (Fig. 2a and 2b). By

measuring the length along axial or transverse direction, we found that axial length decreased rapidly during the first 30 min, while transverse length steadily increased over 90 min (Fig. 2c). Consistent with the changes in length, spreading area decreased during the first 30 min then gradually recovered over the following 60 min (Fig. 2d). These observations indicated that stretching-induced reorientation involved a rapid axial shortening phase and a steady transverse elongation phase.

Distinct Shape Responses during Stretching and Relaxation Phases

The above observations suggested that cellular responses to cyclic stretching may involve distinct protrusive/retractive responses in a spatially/temporally dependent manner, while the reorientation may represent a cumulative result of incremental shape changes. We, therefore, applied difference imaging as a sensitive means for detecting local changes in cell area (Fig. 3a). We first examined the response to a single pulse of stretching for 10s by generating difference images before and after stretching, during stretching, and during post-stretching relaxation (Fig. 3b). To compare the activities along axial and transverse directions, we further divided each cell into two axial and two transverse quadrants (Fig. 3a).

Difference images taken during relaxation showed predominantly transverse protrusions (Fig. 3b), which were most prominent during the first 10 s post stretching then decreased rapidly (Fig. 3b and 3c). In contrast, difference images during stretching showed only baseline activities similar to those of unstretched cells, while difference images immediately before and after stretching showed prominently retractions along both axial and transverse directions (Fig. 3c), suggesting that retraction took place immediately after the release of stretching. Decreasing the duration of stretching from 10 s to 1 s did not significantly decrease the extent of retraction but reduced the

subsequent transverse protrusions and the difference in protrusive activities between transverse and axial directions (Fig. 3c).

We then examined the response to stretching after applying cyclic stretching for up to 45 min at 0.5 Hz (Fig. 4). Interestingly, while protrusive activities of transverse quadrants were maintained following multiple cycles of stretching (Fig. 4, upper left blue bars), protrusions of axial quadrants decreased progressively (Fig. 4, upper right orange bars). In contrast, similar retraction responses were observed along axial and transverse quadrants immediately after the relaxation of stretching, showing strong retraction after a single cycle of stretching but much weaker retraction after additional cycles (Fig. 4). Together, these results explained cyclic stretching-induced reorientation as a cumulative consequence of persistent transverse protrusions coupled with diminishing axial protrusions.

Functional Roles of Myosin II and Microtubules in Cyclic Stretching-Induced Cell Reorientation

Previous studies have implicated actomyosin contractility in cyclic stretching-induced cell reorientation[17,19]. By inhibiting myosin II with blebbistatin, we found that cells became highly branched while showing a weak orientation along the axial direction (Fig. 5a and 5b). In addition, both axial shortening and transverse elongation were suppressed as compared to untreated cells (Fig. 5c), suggesting that actomyosin contractility is directly or indirectly required for both activities.

Since microtubules have been suggested to control cell shape and polarity[25,31,32], we tested the effect of microtubule disassembly on the responses to cyclic stretching. As shown in Fig. 6a and 6b, treatment with nocodazole caused a visibly higher degree of reorientation than controls. Moreover, both axial shortening and transverse elongation reached a greater extent than control

125 cells (Fig. 6c), suggesting that microtubules play a role in tempering the response. Further analyses
126 of the responses during the first 10 s of relaxation after various periods of cyclic stretching
127 revealed that axial protrusion was inhibited transiently after 15min of stretching (Fig. 6d), while
128 transverse protrusion showed an increase after 45 min (Fig. 6d). These effects of nocodazole were
129 consistent with the kinetics of length change as shown in Fig. 6c and implicated a microtubule-
130 mediated mechanism that affects protrusive activities in a location-dependent manner.

Discussion

Although cellular response to cyclic stretching has been studied for decades due to its physiological importance, the transverse reorientation as observed for adherent cells seems counterintuitive. A serious limitation has been the reliance on endpoint analysis in most studies, such that little is known about the dynamic events responsible for the reorientation. In the present study, we have developed a novel cell stretcher based on a motorized microscope stage that allows the recording of live cells in synchrony with cycles of stretching and relaxation. The study was further facilitated by the nearly ideal elastic property of PAA substrates, and by the use of difference imaging for detecting minute changes in cell shape in response to stretching or relaxation.

We found that the response to cyclic stretching took place via an early phase that lasted for 30-45 min, when the reorientation involved primarily net axial retraction, followed by a late phase when the reorientation involved primarily net transverse extension (Fig. 2c). This late phase of extension is similar to the lagged increase in traction forces along the transverse direction as reported previously[33]. In addition, the response to each stretching cycle involved no significant response during stretching, immediate retraction upon relaxation, and protrusion that lasted for 10-20s during the ensuing relaxation (Fig. 3c and Fig. 4). Retractive and protrusive activities showed distinct temporal and spatial patterns. Retraction was global but its magnitude decayed after a few cycles. In contrast, protrusion was more localized and persistent along the transverse direction, while axial protrusions diminished gradually over 30 min (Fig. 4). Together, these events explained not only the reorientation but also the transient decrease in cell area during the first 30 min (Fig. 2e).

153 The key role of relaxation phase in cyclic-stretching-induced reorientation provided a simple
154 answer to the puzzling difference between the responses to cyclic and static stretching, where
155 the reorientation was axial and too slow to be captured during the 1-10 s of stretching in the
156 present cyclic regimen[1,27,28,34]. The requirement of relaxation for reorientation may also explain
157 the dependence of the responses on the waveform of stretching; triangular waves were found to
158 elicit much weaker responses than rectangular or trapezoid waves of a similar peak magnitude.
159 We suspect that while rectangular and trapezoid waves contain discrete periods of relaxation to
160 support transverse elongation, relaxation in triangular waves is gradual and total relaxation is too
161 brief to allow much shape change[10,30].

162 The present relationship between retraction and protrusion may be similar to that in the
163 process of "retraction induced protrusion", where tail retraction was followed by frontal
164 protrusion at the opposite end[32,35,36]. Similarly, symmetry breaking that initiates polarized cell
165 migration typically starts with the formation of a retracting tail, followed by protrusion at the
166 front[37,38]. All these activities may represent a common mechanism of retraction at one end
167 triggering protrusion signals at a distal end. Supporting this hypothesis, we showed that the
168 inhibition of myosin II with blebbistatin suppressed not only axial retraction but also transverse
169 extension (Fig. 5), causing cells to orient along the axial direction possibly as a passive response
170 to stretching[17,19].

171 Previous investigations of the role of microtubules in cell reorientation upon cyclic stretching
172 have yielded conflicting results[19,39-41]. As microtubules are required for establishing cell polarity
173 and directional cell migration[25,41,42], we suspect that they may play a role in coordinating
174 differential transverse and axial extensions, such that their disassembly may eliminate the
175 difference and inhibit cell reorientation. Surprisingly, the disassembly of microtubules caused an

enhancement of cyclic stretching-induced reorientation through the enhancement of both axial retraction and transverse extension (Fig. 6). A possible explanation is that, as microtubules are known to suppress cell contractility[43], disassembly of microtubules may promote stretching-induced retraction and downstream events. A second, non-mutually exclusive possibility is that microtubules, as relatively rigid structures, may be aligned by stretching to generate anisotropic resistance to retraction[41]. Disassembly of microtubules may decrease this resistance to facilitate axial retraction. A third possibility is that retraction signals may be generated at axial ends then transported via microtubules to cause global retractions. Inhibition of microtubules would then cause retraction signals to accumulate at axial ends, enhancing axial retraction while allowing more extensions elsewhere (Supplementary Fig. 3). This hypothetical mechanism is therefore complementary to the local-excitation/global-inhibition (LEGI) mechanism proposed for polarized cell migration[44,45], where microtubules were assumed to transport retraction signals away from the front to create a stable tail while protrusion signals were localized and self-amplified at the front[25].

In summary, the present results suggest that cyclic stretching induces two complementary events during the relaxation phase—an immediate retraction that decays after the first several cycles of stretching, and a slower but more persistent protrusion along the transverse direction. Reorientation represents a cumulative result of stepwise axial retractions and transverse extension at each cycle (Fig. 7). In addition, microtubules may play a role in coordinating the activities between different regions, similar to their proposed role during directional cell migration.

Materials and Methods

Cell Culturing and Pharmacological Treatment. NRK-52E rat kidney epithelial cells (ATCC® CRL-1571™, Manassas, VA) were maintained at 37 °C with 5% (v/v) CO_2 in Dulbecco's modified Eagle's medium (DMEM; Life Technologies, Carlsbad, CA) supplemented with 10%(v/v) fetal bovine serum (Thermo Scientific, Waltham, MA), 2 mM L-glutamine, 50 µg/ml streptomycin, and 50units/ml penicillin (Life Technologies, Carlsbad, CA). Cells were plated on polyacrylamide (PAA) substrate of the stretcher for 36 h before stretching.

Cells were treated with 5 µM nocodazole (Sigma-Aldrich, St. Louis, MO) for 2 h to induce microtubule depolymerization before the application of uniaxial cyclic stretching. Myosin-II contractility was inhibited by treating cells with 50 µM (-)-blebbistatin (Sigma-Aldrich, St. Louis, MO), prepared by slowly diluting a stock solution of 100 mM in DMSO into warm medium under vigorous stirring followed by filtration with a 0.22 µm filter.

Preparation of Cell Stretcher. The stretcher contained a sheet of PAA gel 7.5 mm x 5 mm x 0.4 mm in dimension, one end of which was bonded to a glass coverslip while the opposite end was attached to a handle for anchorage. To prepare the PAA gel, a glass coverslip (45 x 50 mm^2 No. 2; Fisher Scientific) was activated at one end with Bind-Silane (GE Healthcare, Waukesha, WI) for bonding PAA and the remaining area was treated with water-repellant Rain-X® or Repel-Silane (GE Healthcare Life Science) to prevent the adhesion of PAA to the glass (Supplementary Fig. 1g). A casting chamber was then assembled with the activated coverslip, a handle made of a PDMS block attached to a bind-silane treated coverslip (Supplementary Fig. 1h), and a top coverslip micropatterned with gelatin (Supplementary Fig. 1f, 1i, and 1k) [46]. A solution of 10% acrylamide (Bio-Rad, Hercules, CA), 0.3% bis-acrylamide (Bio-Rad, Hercules, CA), 0.001% (w/v) ammonium persulfate (Sigma Aldrich, St. Louis, MO), and 0.004% (v/v) N,N,N',N'-tetramethylene-1,2-diamine (TEMED, Bio-Rad, Hercules, CA) was injected into the chamber and allowed to polymerize for 45min. The coverslip with PAA substrate was then attached with vacuum grease to an acrylic block with a hole, to form a culture chamber with stretchable substrate (Fig. 1B).

Micropatterned coverslips were prepared as described previously[47]. To micropattern coverslips with gelatin, PDMS stamps were prepared by polymerizing Silgard 184 (Dow, Midland, Michigan) on a photoresist mold (Supplementary Fig. 1a-b; SPR 220, MicroChem, Round Rock, TX), and coated with 0.1%(w/v) periodate-activated gelatin (Supplementary Fig. 1c, 3.5 mg/mL sodium m-periodate, Sigma-Aldrich, St. Louis, MO), before pressing on a 25x25 mm^2 No. 1.5 coverslip to transfer the pattern (Supplementary Fig. 1d-e).

Strain Analysis. Fluorescent latex beads (0.2µm diameter, red, polystyrene; Molecular Probes, Carlsbad, CA) were added to the acrylamide solution for revealing the ECM micropattern. Microcontact-printed squares 50x50 μm^2 in area were used for visualizing the strain of the PAA gel in response to the stress induced by stage movement. Deformation of the square pattern was imaged in response to stage movements calculated to stretch the gel by 5%, 10%, 15%, or 20%. Fluorescent images were analyzed with ImageJ (National Institutes of Health, Bethesda, MD), and the length and width of the square as a function of stretching distance was analyzed with linear regression. Residual strain upon relaxation was determined by measuring the offset of local marks before and after stretching.

Microscopy and Live-cell Imaging. The microscope was covered with a plastic enclosure to serve as an incubator, wherein the temperature and CO_2 concentration was maintained for cell viability.

Phase-contrast images of cells were collected with a Zeiss Axiovet 200M microscope using a 40x N.A. 0.55 phase contrast dry objective lens. The microscope was equipped with a high-precision motorized stage (MS-2000 XYZ, Applied Scientific Instrumentation, Eugene, OR). Before stretching, a rod on a micromanipulator was used for fixing the position of the handle attached to the PAA sheet, while the coverslip moved back and forth with the motorized stage. Custom software was used for controlling and coordinating stage movement and image acquisition.

Analysis of Cell Orientation, Cell Length, and Protrusion Activities. Cell outline was drawn manually using ImageJ for determining the spreading area. The outline was then fit with an ellipse, and the orientation index was determined as $cos2\vartheta$ where ϑ is the long axis of the ellipse. Perfect alignment parallel and perpendicular to the direction of stretching was indicated by an orientation index of 1 and -1, respectively. Cell outline was also fitted with a rectangular to determine the cell transverse/axial length as the width/length of the rectangle. Protrusion and retraction activities were calculated using the difference of consecutive images, using a custom MATLAB program. Areas of net protrusion or retraction were normalized against the average cell spreading area.

Statistics Analysis. All the data were evaluated from at least three independent experiments conducted on different stretchers. Orientation index ($cos2\vartheta$) was statistically analyzed by the Friedman test in conjunction with Dunn's multi-comparison test, since the data were non-normal distributed. Statistical significance of the difference in cell length at different points of a time sequence was determined by repeated one-way ANOVA, while the comparisons of cells under diverse conditions were conducted using simple *t*-test. Mixed model two-way ANOVA with Tukey's multi-comparisons test was used to determine the statistical difference of cell retraction following various period of cyclic stretching.

References

1 Lo, C. M., Wang, H. B., Dembo, M. & Wang, Y. L. Cell movement is guided by the rigidity of the substrate. *Biophys J* **79**, 144-152, doi:10.1016/S0006-3495(00)76279-5 (2000).

2 Throm Quinlan, A. M., Sierad, L. N., Capulli, A. K., Firstenberg, L. E. & Billiar, K. L. Combining dynamic stretch and tunable stiffness to probe cell mechanobiology in vitro. *PLoS One* **6**, e23272, doi:10.1371/journal.pone.0023272 (2011).

3 Shafieyan, Y. & Hinz, B. Signs of stress on soft surfaces : A commentary on: Cui, Y., F.M. Hameed, B. Yang, K. Lee, C.Q. Pan, S. Park, and M. Sheetz. 2015. Cyclic stretching of soft substrates induces spreading and growth. Nat Commun. 6:6333. *J Cell Commun Signal* **9**, 305-307, doi:10.1007/s12079-015-0305-7 (2015).

4 Rosowski, K. A. *et al.* Vinculin and the mechanical response of adherent fibroblasts to matrix deformation. *Sci Rep* **8**, 17967, doi:10.1038/s41598-018-36272-9 (2018).

5 Balachandran, K., Sucosky, P., Jo, H. & Yoganathan, A. P. Elevated cyclic stretch induces aortic valve calcification in a bone morphogenic protein-dependent manner. *Am J Pathol* **177**, 49-57, doi:10.2353/ajpath.2010.090631 (2010).

6 Kurpinski, K., Park, J., Thakar, R. G. & Li, S. Regulation of vascular smooth muscle cells and mesenchymal stem cells by mechanical strain. *Mol Cell Biomech* **3**, 21-34 (2006).

7 Buck, R. C. Reorientation response of cells to repeated stretch and recoil of the substratum. *Exp Cell Res* **127**, 470-474, doi:10.1016/0014-4827(80)90456-5 (1980).

8 Ives, C. L., Eskin, S. G. & McIntire, L. V. Mechanical effects on endothelial cell morphology: in vitro assessment. *In Vitro Cell Dev Biol* **22**, 500-507, doi:10.1007/BF02621134 (1986).
9 Jungbauer, S., Gao, H., Spatz, J. P. & Kemkemer, R. Two characteristic regimes in frequency-dependent dynamic reorientation of fibroblasts on cyclically stretched substrates. *Biophys J* **95**, 3470-3478, doi:10.1529/biophysj.107.128611 (2008).
10 Tondon, A., Hsu, H. J. & Kaunas, R. Dependence of cyclic stretch-induced stress fiber reorientation on stretch waveform. *J Biomech* **45**, 728-735, doi:10.1016/j.jbiomech.2011.11.012 (2012).
11 Wang, J. H., Goldschmidt-Clermont, P., Wille, J. & Yin, F. C. Specificity of endothelial cell reorientation in response to cyclic mechanical stretching. *J Biomech* **34**, 1563-1572, doi:10.1016/s0021-9290(01)00150-6 (2001).
12 Roshanzadeh, A. *et al.* Mechanoadaptive organization of stress fiber subtypes in epithelial cells under cyclic stretches and stretch release. *Sci Rep* **10**, 18684, doi:10.1038/s41598-020-75791-2 (2020).
13 Lee, E. *et al.* Transplantation of cyclic stretched fibroblasts accelerates the wound-healing process in streptozotocin-induced diabetic mice. *Cell Transplant* **23**, 285-301, doi:10.3727/096368912X663541 (2014).
14 Rolin, G. L. *et al.* In vitro study of the impact of mechanical tension on the dermal fibroblast phenotype in the context of skin wound healing. *J Biomech* **47**, 3555-3561, doi:10.1016/j.jbiomech.2014.07.015 (2014).
15 Matsumoto, T. *et al.* Mechanical strain regulates endothelial cell patterning in vitro. *Tissue Eng* **13**, 207-217, doi:10.1089/ten.2006.0058 (2007).
16 Fernandez-Gonzalez, R. & Zallen, J. A. Oscillatory behaviors and hierarchical assembly of contractile structures in intercalating cells. *Phys Biol* **8**, 045005, doi:10.1088/1478-3975/8/4/045005 (2011).
17 Greiner, A. M., Chen, H., Spatz, J. P. & Kemkemer, R. Cyclic tensile strain controls cell shape and directs actin stress fiber formation and focal adhesion alignment in spreading cells. *PLoS One* **8**, e77328, doi:10.1371/journal.pone.0077328 (2013).
18 Goldyn, A. M., Rioja, B. A., Spatz, J. P., Ballestrem, C. & Kemkemer, R. Force-induced cell polarisation is linked to RhoA-driven microtubule-independent focal-adhesion sliding. *J Cell Sci* **122**, 3644-3651, doi:10.1242/jcs.054866 (2009).
19 Goldyn, A. M., Kaiser, P., Spatz, J. P., Ballestrem, C. & Kemkemer, R. The kinetics of force-induced cell reorganization depend on microtubules and actin. *Cytoskeleton (Hoboken)* **67**, 241-250, doi:10.1002/cm.20439 (2010).
20 Faust, U. *et al.* Cyclic Stress at mHz Frequencies Aligns Fibroblasts in Direction of Zero Strain. *Plos One* **6**, doi:ARTN e2896310.1371/journal.pone.0028963 (2011).
21 Cirka, H. *et al.* Active Traction Force Response to Long-Term Cyclic Stretch Is Dependent on Cell Pre-stress. *Biophys J* **110**, 1845-1857, doi:10.1016/j.bpj.2016.02.036 (2016).
22 Chen, C. *et al.* Fluidization and resolidification of the human bladder smooth muscle cell in response to transient stretch. *PLoS One* **5**, e12035, doi:10.1371/journal.pone.0012035 (2010).
23 Livne, A., Bouchbinder, E. & Geiger, B. Cell reorientation under cyclic stretching. *Nat Commun* **5**, 3938, doi:10.1038/ncomms4938 (2014).

24 Stamenovic, D., Krishnan, R., Canovic, E. P. & Smith, M. L. As the endothelial cell reorients, its tensile forces stabilize. *J Biomech* **105**, 109770, doi:10.1016/j.jbiomech.2020.109770 (2020).

25 Zhang, J., Guo, W. H. & Wang, Y. L. Microtubules stabilize cell polarity by localizing rear signals. *Proc Natl Acad Sci U S A* **111**, 16383-16388, doi:10.1073/pnas.1410533111 (2014).

26 Kaunas, R., Nguyen, P., Usami, S. & Chien, S. Cooperative effects of Rho and mechanical stretch on stress fiber organization. *Proc Natl Acad Sci U S A* **102**, 15895-15900, doi:10.1073/pnas.0506041102 (2005).

27 Munevar, S., Wang, Y. L. & Dembo, M. Regulation of mechanical interactions between fibroblasts and the substratum by stretch-activated Ca2+ entry. *J Cell Sci* **117**, 85-92, doi:10.1242/jcs.00795 (2004).

28 Katsumi, A. *et al.* Effects of cell tension on the small GTPase Rac. *J Cell Biol* **158**, 153-164, doi:10.1083/jcb.200201105 (2002).

29 Liu, B. *et al.* Role of cyclic strain frequency in regulating the alignment of vascular smooth muscle cells in vitro. *Biophys J* **94**, 1497-1507, doi:10.1529/biophysj.106.098574 (2008).

30 Nagayama, K., Kimura, Y., Makino, N. & Matsumoto, T. Strain waveform dependence of stress fiber reorientation in cyclically stretched osteoblastic cells: effects of viscoelastic compression of stress fibers. *Am J Physiol Cell Physiol* **302**, C1469-1478, doi:10.1152/ajpcell.00155.2011 (2012).

31 Meiring, J. C. M., Shneyer, B. I. & Akhmanova, A. Generation and regulation of microtubule network asymmetry to drive cell polarity. *Curr Opin Cell Biol* **62**, 86-95, doi:10.1016/j.ceb.2019.10.004 (2020).

32 Kaverina, I. *et al.* Enforced polarisation and locomotion of fibroblasts lacking microtubules. *Curr Biol* **10**, 739-742, doi:10.1016/s0960-9822(00)00544-3 (2000).

33 Krishnan, R. *et al.* Fluidization, resolidification, and reorientation of the endothelial cell in response to slow tidal stretches. *Am J Physiol Cell Physiol* **303**, C368-375, doi:10.1152/ajpcell.00074.2012 (2012).

34 Chen, Y., Pasapera, A. M., Koretsky, A. P. & Waterman, C. M. Orientation-specific responses to sustained uniaxial stretching in focal adhesion growth and turnover. *Proc Natl Acad Sci U S A* **110**, E2352-2361, doi:10.1073/pnas.1221637110 (2013).

35 Chen, W. T. Induction of spreading during fibroblast movement. *J Cell Biol* **81**, 684-691, doi:10.1083/jcb.81.3.684 (1979).

36 Guo, W. H. & Wang, Y. L. A three-component mechanism for fibroblast migration with a contractile cell body that couples a myosin II-independent propulsive anterior to a myosin II-dependent resistive tail. *Mol Biol Cell* **23**, 1657-1663, doi:10.1091/mbc.E11-06-0556 (2012).

37 Cramer, L. P. Forming the cell rear first: breaking cell symmetry to trigger directed cell migration. *Nat Cell Biol* **12**, 628-632, doi:10.1038/ncb0710-628 (2010).

38 Yam, P. T. *et al.* Actin-myosin network reorganization breaks symmetry at the cell rear to spontaneously initiate polarized cell motility. *Journal of Cell Biology* **178**, 1207-1221, doi:10.1083/jcb.200706012 (2007).

39 Morioka, M. *et al.* Microtubule dynamics regulate cyclic stretch-induced cell alignment in human airway smooth muscle cells. *PLoS One* **6**, e26384, doi:10.1371/journal.pone.0026384 (2011).

40 Iba, T. & Sumpio, B. E. Morphological response of human endothelial cells subjected to cyclic strain in vitro. *Microvasc Res* **42**, 245-254, doi:10.1016/0026-2862(91)90059-k (1991).
41 Kaverina, I. *et al.* Tensile stress stimulates microtubule outgrowth in living cells. *J Cell Sci* **115**, 2283-2291 (2002).
42 Vasiliev, J. M. *et al.* Effect of colcemid on the locomotory behaviour of fibroblasts. *J Embryol Exp Morphol* **24**, 625-640 (1970).
43 Takeda, M., Sami, M. M. & Wang, Y. C. A homeostatic apical microtubule network shortens cells for epithelial folding via a basal polarity shift. *Nat Cell Biol* **20**, 36-45, doi:10.1038/s41556-017-0001-3 (2018).
44 Parent, C. A. & Devreotes, P. N. A cell's sense of direction. *Science* **284**, 765-770, doi:10.1126/science.284.5415.765 (1999).
45 Xiong, Y., Huang, C. H., Iglesias, P. A. & Devreotes, P. N. Cells navigate with a local-excitation, global-inhibition-biased excitable network. *Proc Natl Acad Sci U S A* **107**, 17079-17086, doi:10.1073/pnas.1011271107 (2010).
46 Rape, A. D., Guo, W. H. & Wang, Y. L. The regulation of traction force in relation to cell shape and focal adhesions. *Biomaterials* **32**, 2043-2051, doi:10.1016/j.biomaterials.2010.11.044 (2011).
47 Zhang, J., Guo, W. H., Rape, A. & Wang, Y. L. Micropatterning cell adhesion on polyacrylamide hydrogels. *Methods Mol Biol* **1066**, 147-156, doi:10.1007/978-1-62703-604-7_13 (2013).

Acknowledgments
This work was supported by NIH grants R01 GM118998 and R35 GM136345.

Author Contributions
J.-C.L. designed and performed the experiments, analyzed the data, and drafted the manuscript; Y.-L.W. assisted with experimental design, data analysis and data interpretation, and edited the manuscript.

Competing Interests
The authors declare no conflict of interest.

Figures

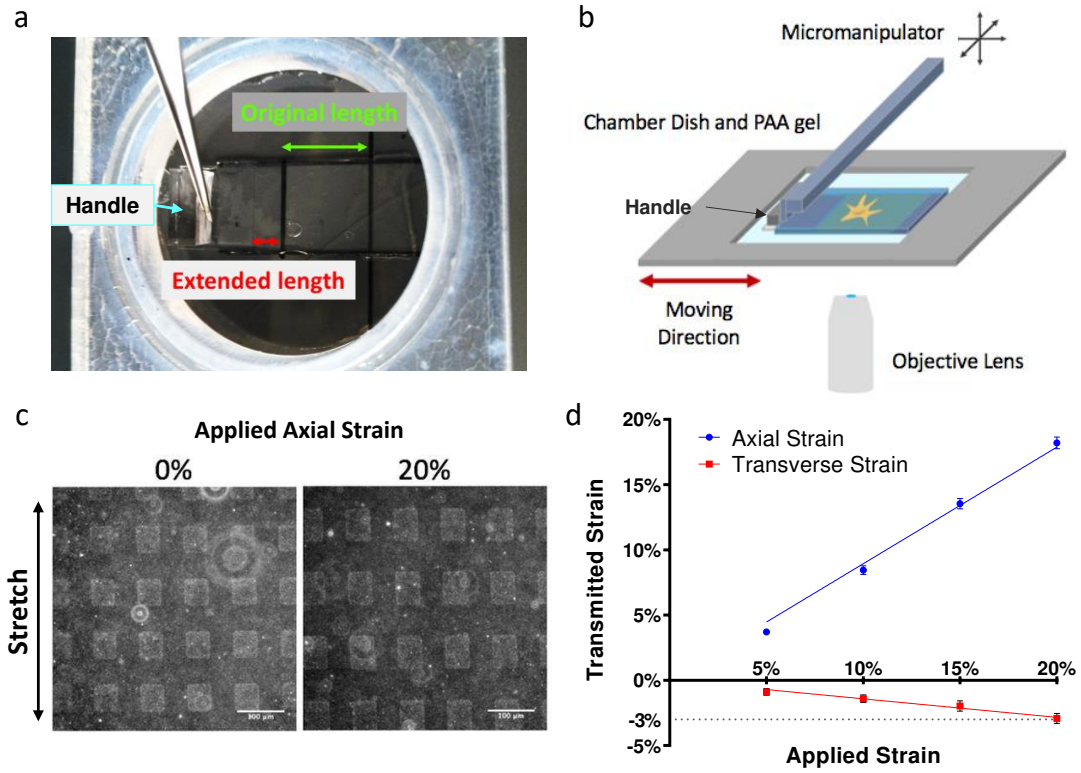

Figure 1. Cell stretcher built upon a microscope with a motorized stage. (**a**) The opposite ends of an elastic PAA gel are covalently bonded to a supporting coverslip and a handle, respectively. The stretcher is mounted on an acrylic holder to form a cell culture chamber and placed on the motorized microscope stage. (**b**) After locating the region of interest, the handle of the gel is anchored by a rod mounted on a micromanipulator. Back and forth movements of the stage cause cyclic stretching of the gel. (**c**) Micropatterned squares on the gel surface, 50 x 50 μm^2 in size and 50 µm apart from each other, are revealed by the concentration of fluorescent beads underneath protein-coated regions during microcontact printing. (**d**) Axial and transverse strains of the gel, as measured by the deformation of the square pattern, vary linearly with calculated strains. However, axial strain is >6 times larger than transverse strain. (Scale bar, 100 µm; n = 5, Mean ± SEM.)

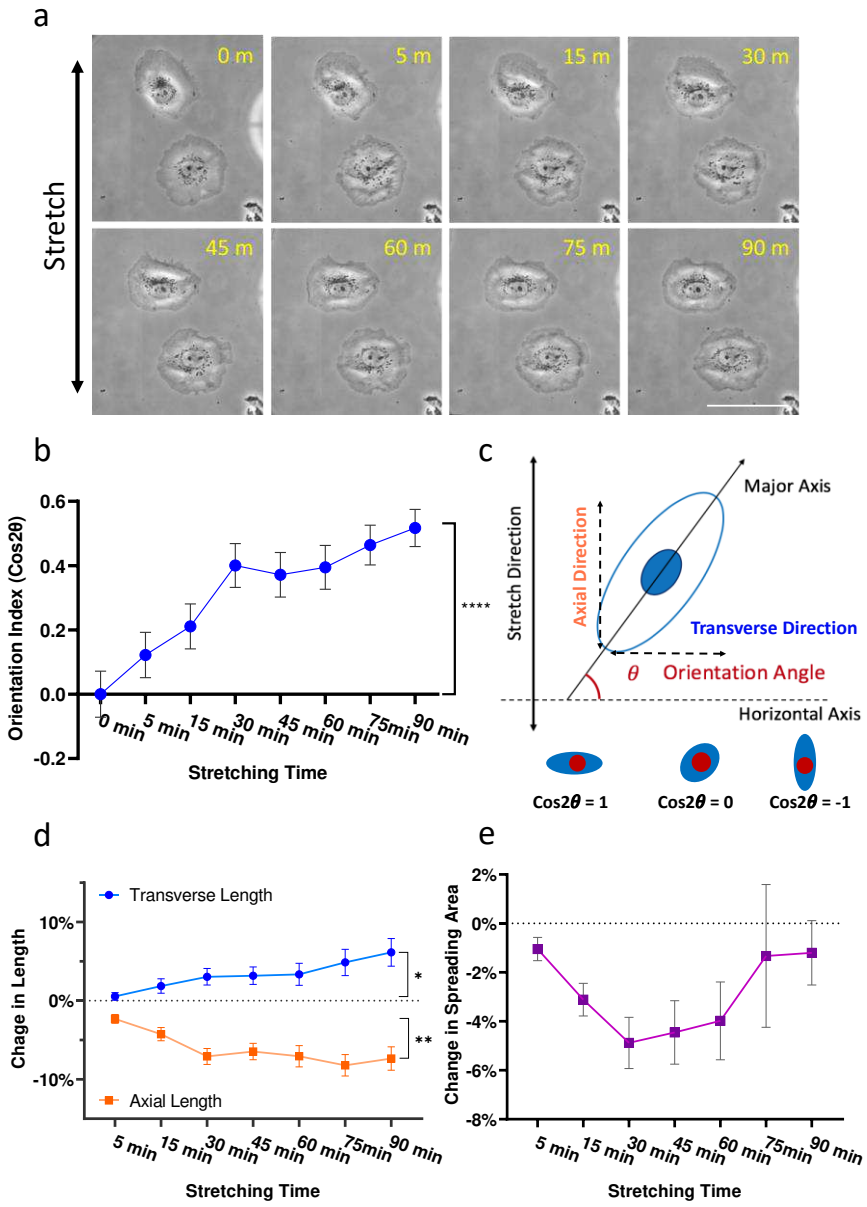

Figure 2. Changes in shape, orientation, and area of NRK-52E epithelial cells in response to uniaxial cyclic stretching. (**a**) Isolated NRK-52E cells show visible shape change and reorientation perpendicular to the direction of stretching over 90min of stretching (scale bar, 100 µm). (**b**) Orientation index is calculated as $cos2\theta$ where θ is the angle between the major axis of the cell and the transverse direction. Transverse orientation, detectable as early as 5 min after the initiation of cyclic stretching, increases steadily over a period of 90 min. (**c and d**) Corresponding changes in cell length along axial and transverse directions, and in spreading area, are also observed during 90 min of cyclic stretching. Shape change is driven primarily by shortening along the axial direction during the first 30-45 min of cyclic stretching, in conjunction with a slow but continuous increase in transverse length and recovery in spreading area between 45 and 90 min (**c and d**). The two distinct phases before and after 30-45 min are indicated by vertical dashed lines. (* $p < 0.05$; ** $p < 0.01$; **** $p < 0.0001$; n = 82, Mean ± SEM.)

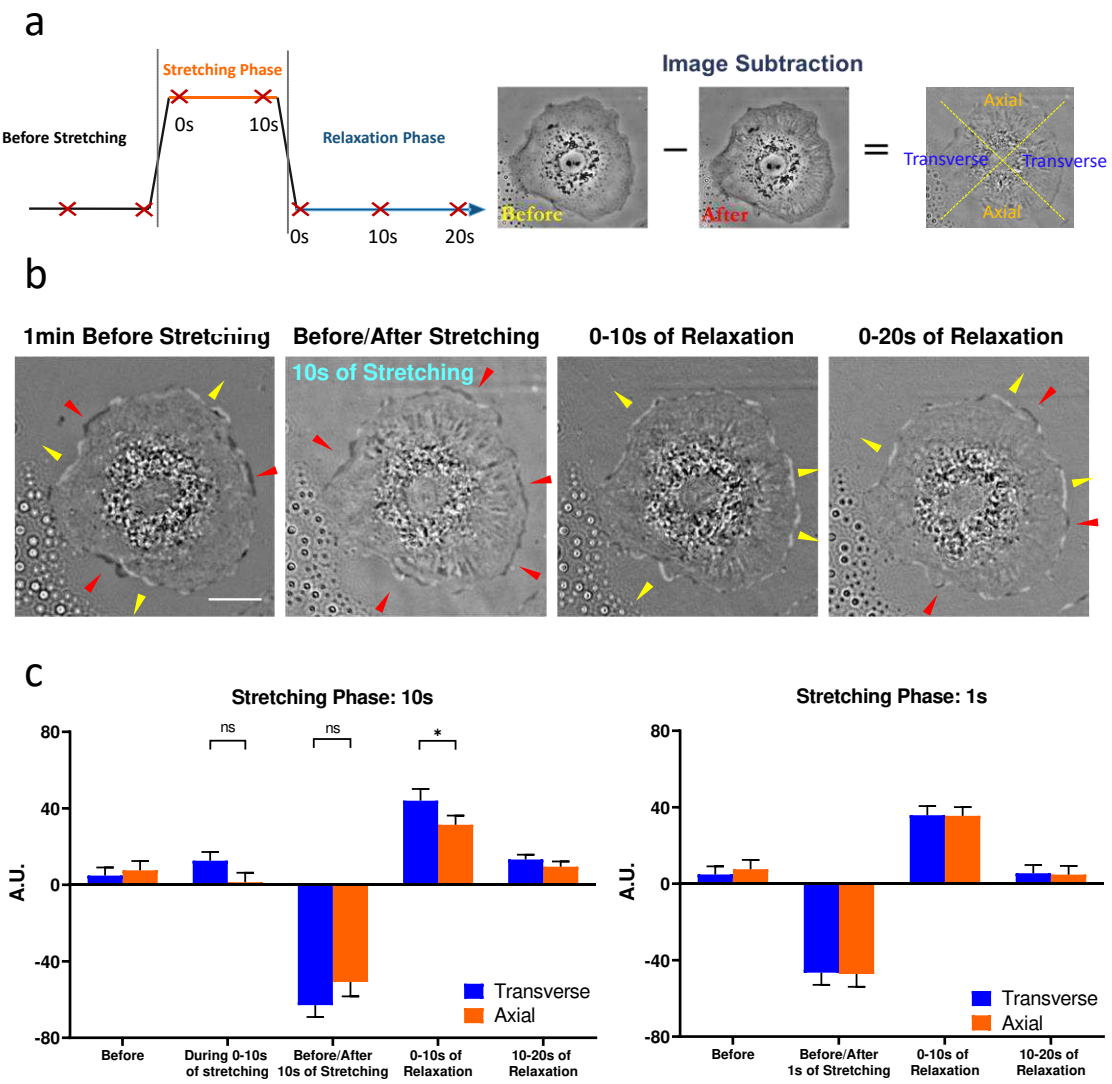

Figure 3. Distinct protrusive and retractive responses to a single pulse of stretching. (**a**) Images are collected before, during, and after stretching, as indicated by red crosses (left diagram). Shape changes are detected by difference imaging between consecutive images. Each cell is divided into two axial and two transverse quadrants, by drawing two diagonal lines at the centroid (right diagram). (**b**) Dark (red arrows) and bright (yellow arrows) regions in the difference image indicate retraction and protrusion, respectively. (**c and d**) Before and during 10 s of stretching, cells show only randomly distributed retractions and protrusions, resulting in little net change in peripheral area for transverse or axial quadrants. Strong retractions occur immediately upon relaxation, while protrusions dominate during the following 10 s of relaxation (**b, c**; scale bar, 20 μm). Reducing the duration of stretching to 1s has no significant effect on the extent of retraction but reduces the subsequent transverse extension (n.s. $p>0.05$, * $p<0.05$; n = 20, Mean ± SEM.)

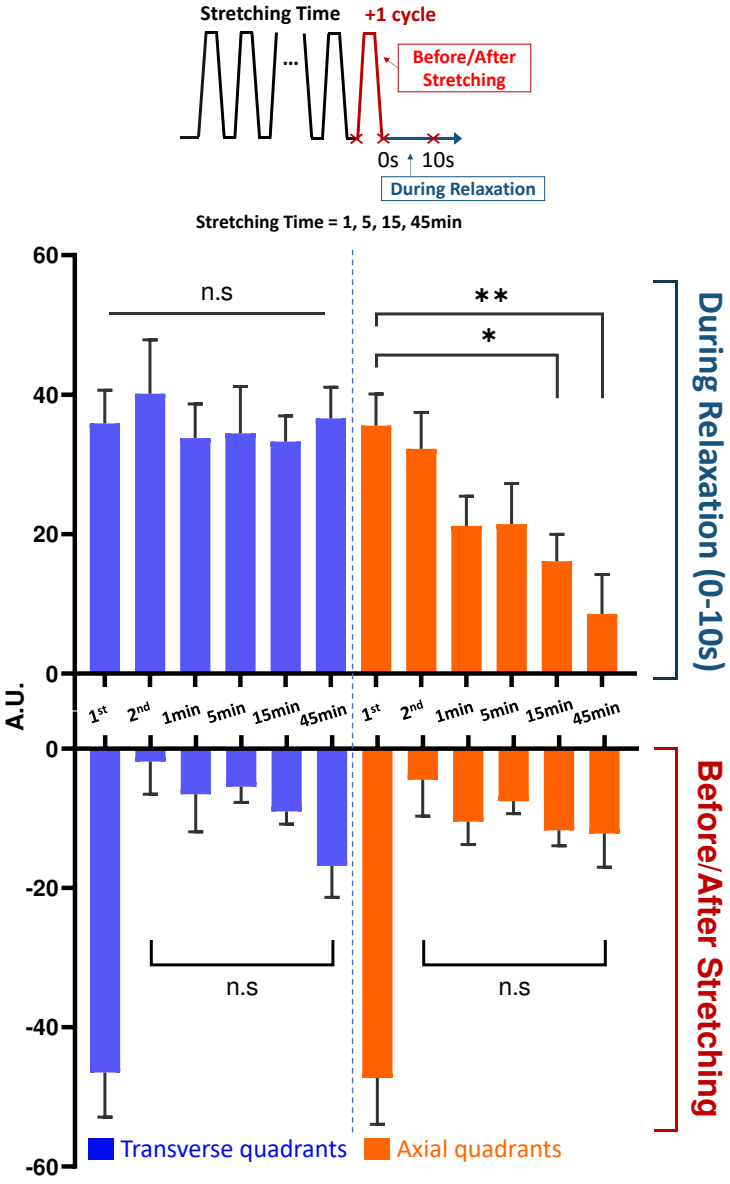

Figure 4. Differential axial and transverse responses following multiple cycles of stretching. Changes in peripheral areas are measured at the 1st cycle, 2nd cycle, and after various periods of cyclic stretching at 0.5 Hz as shown in the diagram, where the timing of image acquisition relative to the stretching cycles is indicated by red crosses. Local retractions or protrusions of different quadrants are then integrated and normalized against the total spreading area to reveal net extension (positive values) or retraction (negative values). Net retraction takes place immediately after stretching (lower graph), while net extension takes place during subsequent 10 s of relaxation (upper graph). Moreover, net extension of axial quadrants decreases progressively with increasing cycles of stretching (top orange), while net extension of transverse quadrants remains constant (top blue). Retraction occurs similarly in all the quadrants, showing a strong response following a single cycle of stretching and a precipitous decrease with additional cycles of stretching (bottom graphs). (* $p < 0.05$; ** $p < 0.01$; n = 16- 20, Mean ± SEM.)

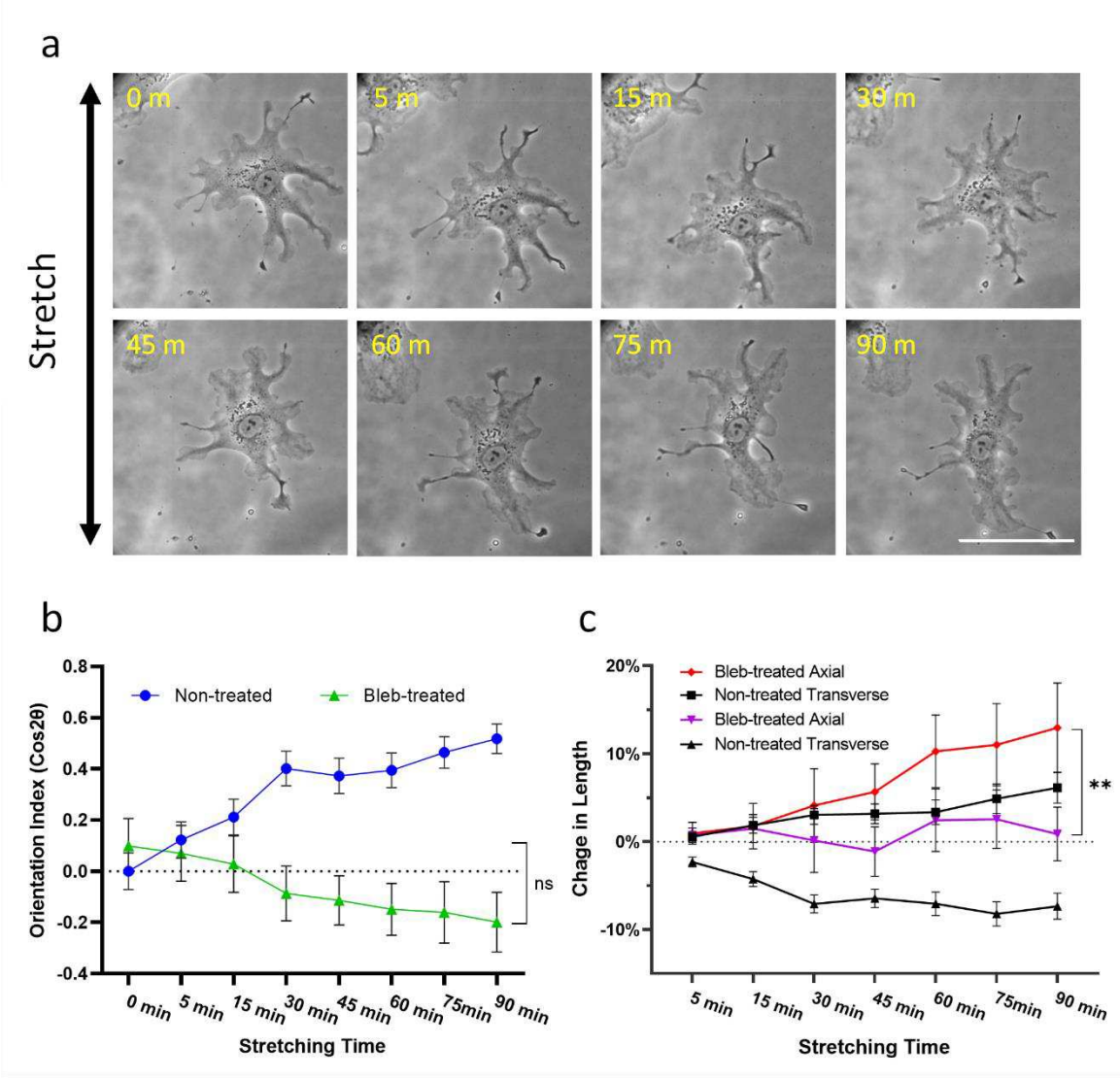

Figure 5. Effect of blebbistatin on cell reorientation and length change in response to cyclic stretching. (**a**) Myosin II activities are inhibited by treating cells with 50 µM blebbistatin for 30 min before applying cyclic stretching. Cells respond by elongating along axial direction (scale bar, 100 µm). (**b**) Unlike control cells, blebbistatin-treated cells show weakly significant axial reorientation. (**c**) The response to blebbistatin involves an increase in axial length and an inhibition of transverse elongation. (n.s. $p > 0.05$, ** $p < 0.01$; n = 46, Mean ± SEM.)

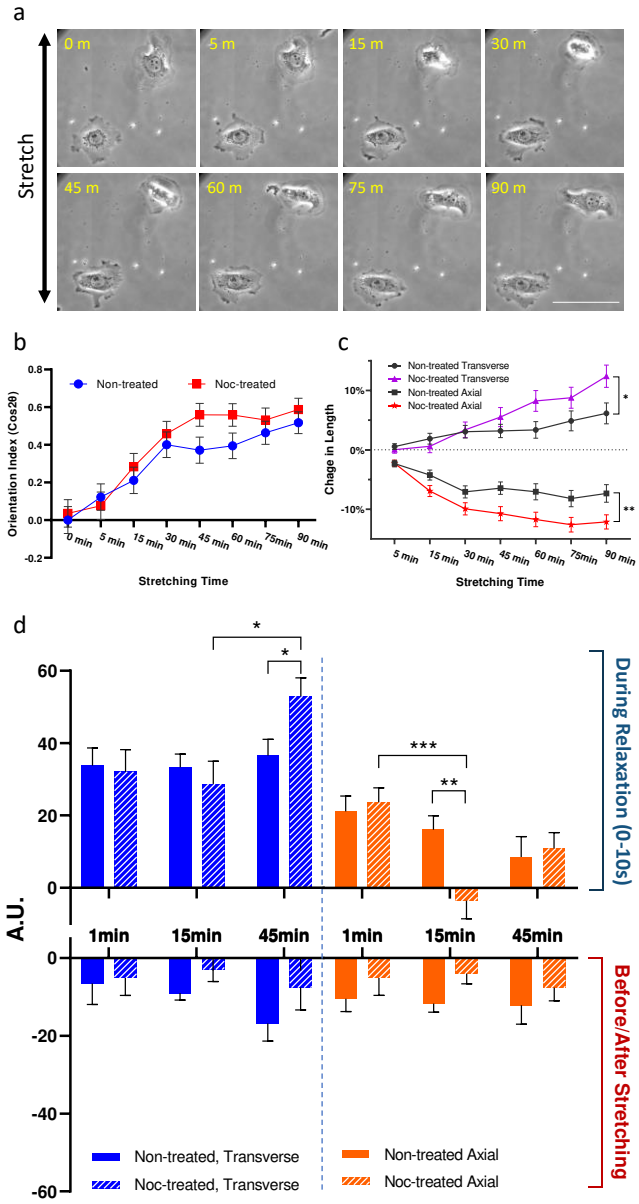

Figure 6. Effects of nocodazole on cell reorientation and length change in response to cyclic stretching. (**a**) Cells, treated with 5µM nocodazole for 2h before applying cyclic stretching, show more pronounced shape change and reorientation than control cells shown in Figure 2. (**b** and **c**) Comparison of control and nocodazole treated cells for reorientation and length change suggests that the effects of nocodazole take place primarily after 30min of cyclic stretching, as an increase in both transverse elongation and axial shortening (* $p < 0.05$; ** $p < 0.01$; n = 98, Mean ± SEM). Similar to the analysis in Fig. 4, changes of peripheral area are measured in nocodazole-treated and control cells. (**d**) Compared to the control (solid bars), nocodazole causes a transient inhibition of axial protrusion after 15 min of cyclic stretching (striped orange bar, upper graph), and a late stimulation of transverse protrusion at 45min (striped blue bar, upper graph). Nocodazole treated cells also show net retraction immediately after stretching (lower graph), similar to control cells. (* $p < 0.05$; ** $p < 0.01$; *** $p < 0.001$; n = 16 - 20, Mean ± SEM).

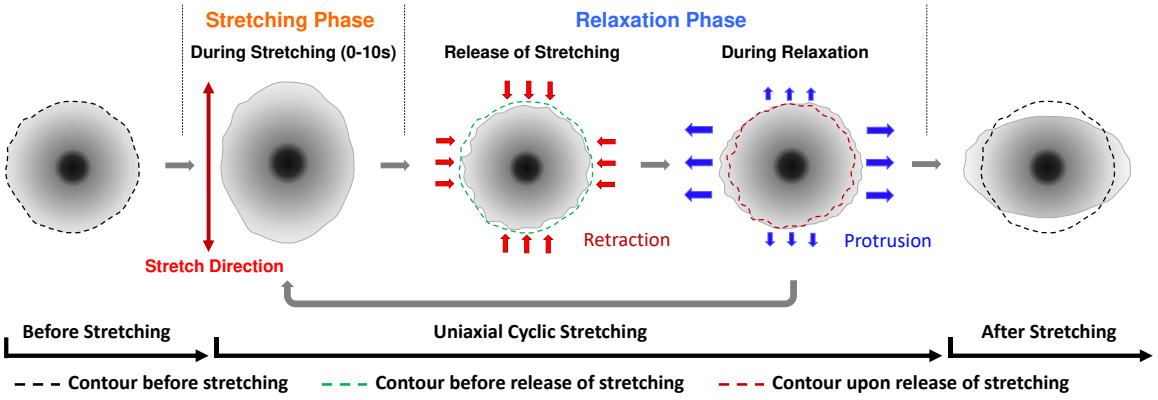

Figure 7. Summary of spatially and temporally dependent protrusion/retraction activities that lead to cell reorientation in response to uniaxial cyclic stretching. Cells (greyscale circle) retract immediately upon the release of stretching (red arrows), followed by progressive extension during the relaxation phase (blue arrows). The effects accumulate upon prolonged cyclic stretching, which leads to the change in cell shape and orientation.

Figures

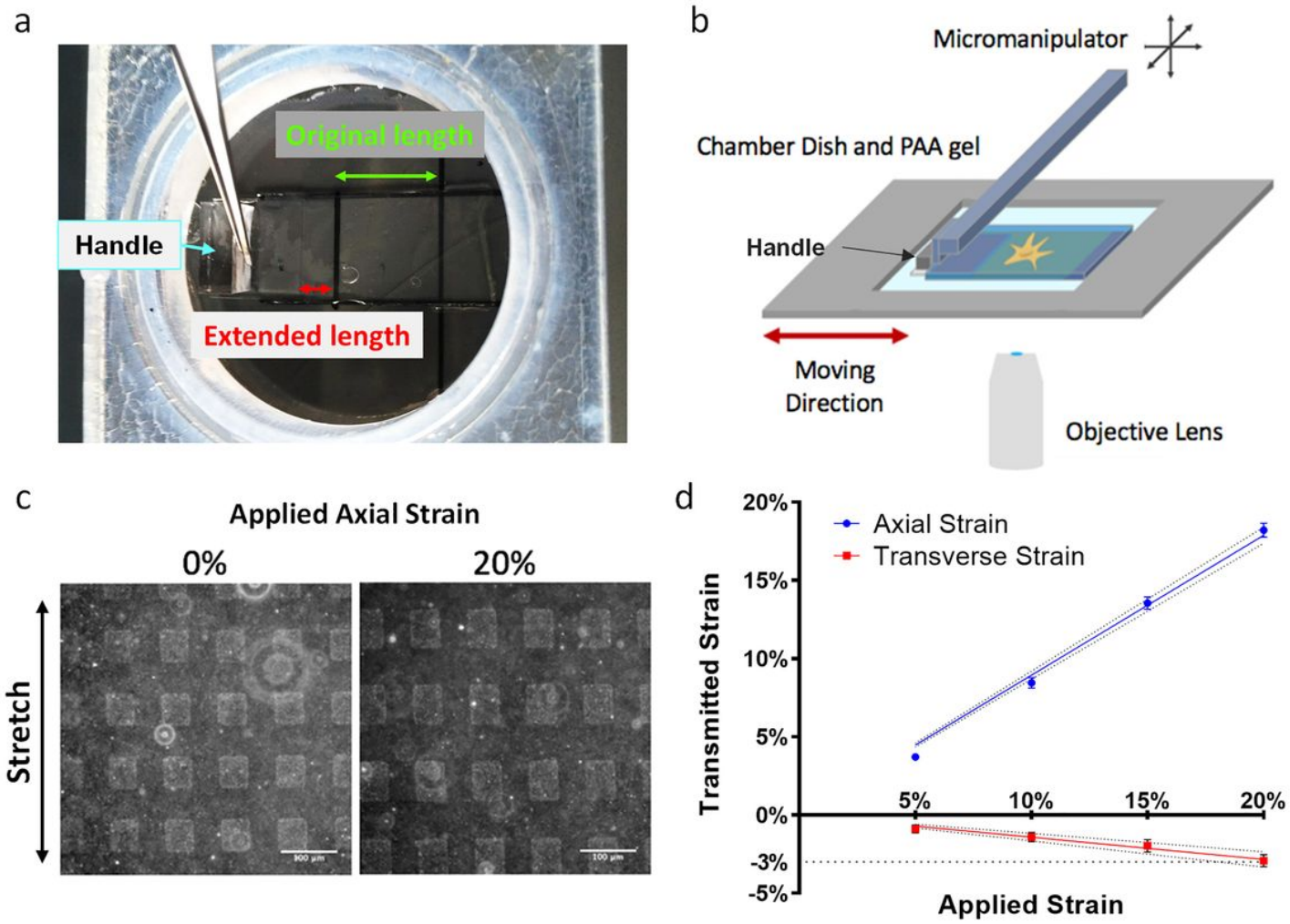

Figure 1

Cell stretcher built upon a microscope with a motorized stage. (a) The opposite ends of an elastic PAA gel are covalently bonded to a supporting coverslip and a handle, respectively. The stretcher is mounted on an acrylic holder to form a cell culture chamber and placed on the motorized microscope stage. (b) After locating the region of interest, the handle of the gel is anchored by a rod mounted on a micromanipulator. Back and forth movements of the stage cause cyclic stretching of the gel. (c) Micropatterned squares on the gel surface, 50 x 50 μm2 in size and 50 μm apart from each other, are revealed by the concentration of fluorescent beads underneath protein-coated regions during microcontact printing. (d) Axial and transverse strains of the gel, as measured by the deformation of the square pattern, vary linearly with calculated strains. However, axial strain is >6 times larger than transverse strain. (Scale bar, 100 μm; n = 5, Mean ± SEM.)

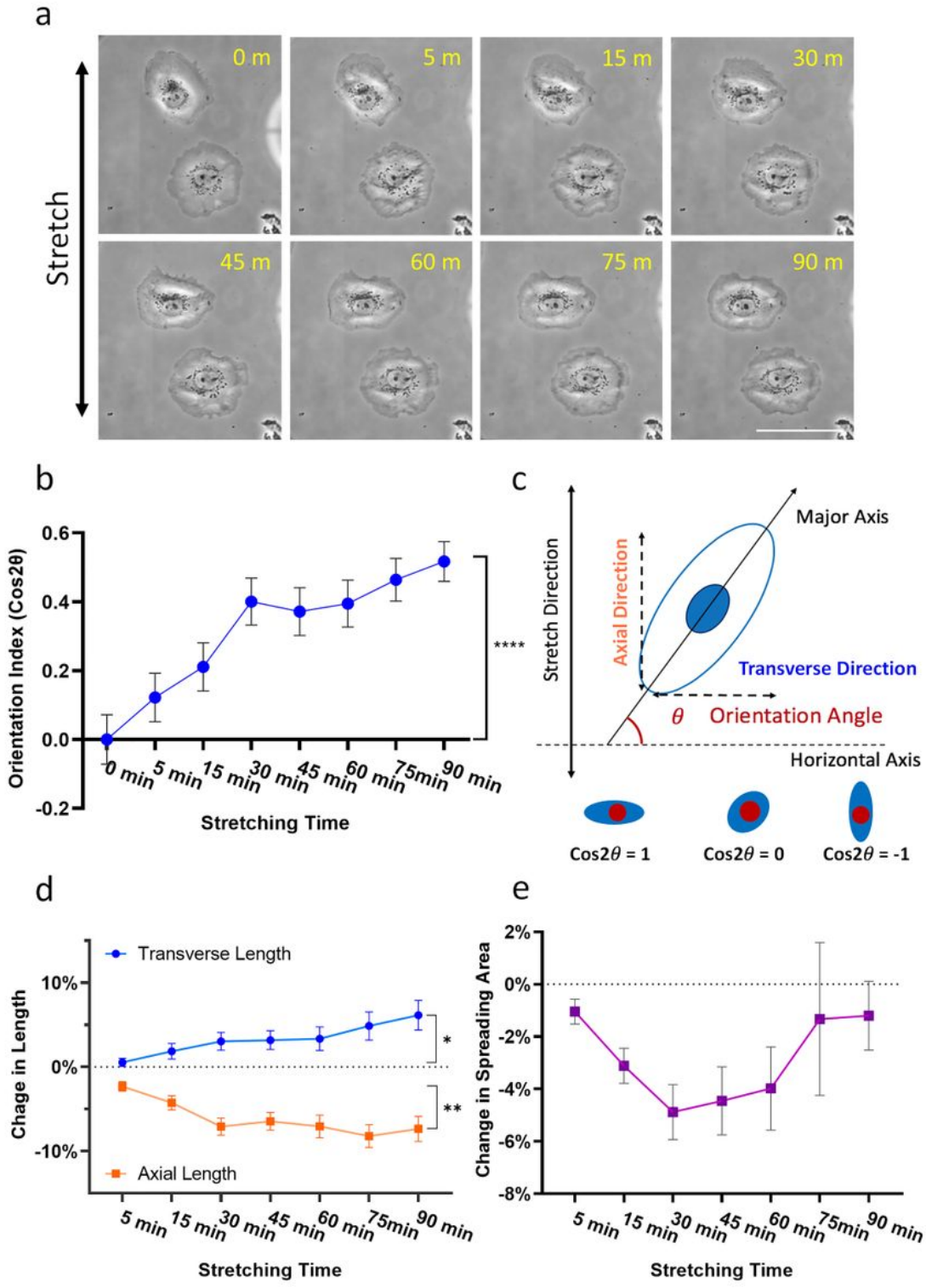

Figure 2

Changes in shape, orientation, and area of NRK-52E epithelial cells in response to uniaxial cyclic stretching. (a) Isolated NRK-52E cells show visible shape change and reorientation perpendicular to the direction of stretching over 90min of stretching (scale bar, 100 μm). (b) Orientation index is calculated as cos2θ where θ is the angle between the major axis of the cell and the transverse direction. Transverse orientation, detectable as early as 5 min after the initiation of cyclic stretching, increases steadily over a

period of 90 min. (c and d) Corresponding changes in cell length along axial and transverse directions, and in spreading area, are also observed during 90 min of cyclic stretching. Shape change is driven primarily by shortening along the axial direction during the first 30-45 min of cyclic stretching, in conjunction with a slow but continuous increase in transverse length and recovery in spreading area between 45 and 90 min (c and d). The two distinct phases before and after 30-45 min are indicated by vertical dashed lines. (* $p < 0.05$; ** $p < 0.01$; **** $p < 0.0001$; n = 82, Mean ± SEM.)

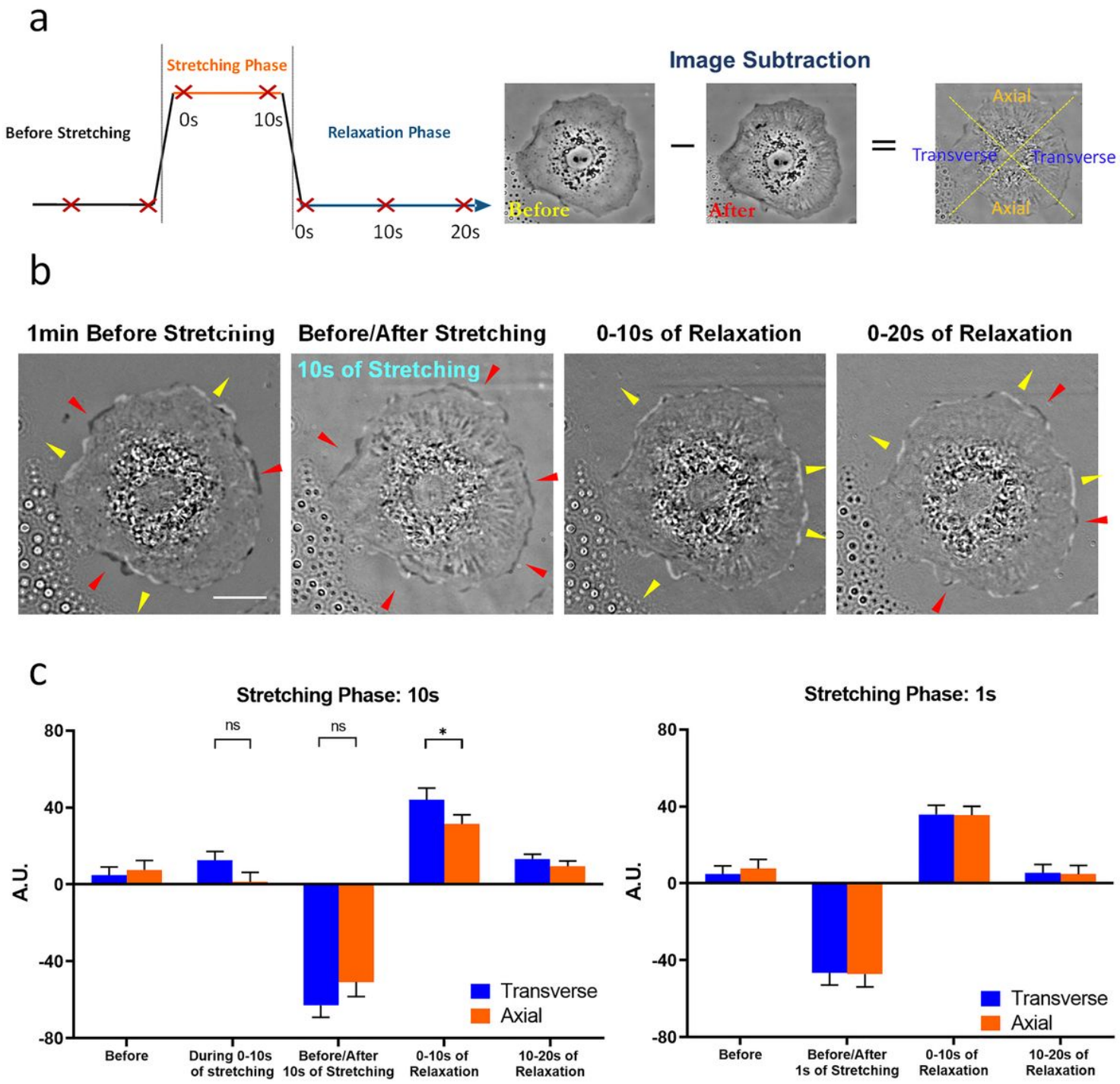

Figure 3

Distinct protrusive and retractive responses to a single pulse of stretching. (a) Images are collected before, during, and after stretching, as indicated by red crosses (left diagram). Shape changes are detected by difference imaging between consecutive images. Each cell is divided into two axial and two transverse quadrants, by drawing two diagonal lines at the centroid (right diagram). (b) Dark (red arrows) and bright (yellow arrows) regions in the difference image indicate retraction and protrusion, respectively. (c and d) Before and during 10 s of stretching, cells show only randomly distributed retractions and protrusions, resulting in little net change in peripheral area for transverse or axial quadrants. Strong retractions occur immediately upon relaxation, while protrusions dominate during the following 10 s of relaxation (b, c; scale bar, 20 μm). Reducing the duration of stretching to 1s has no significant effect on the extent of retraction but reduces the subsequent transverse extension (n.s. $p>0.05$, * $p<0.05$; $n = 20$, Mean ± SEM.)

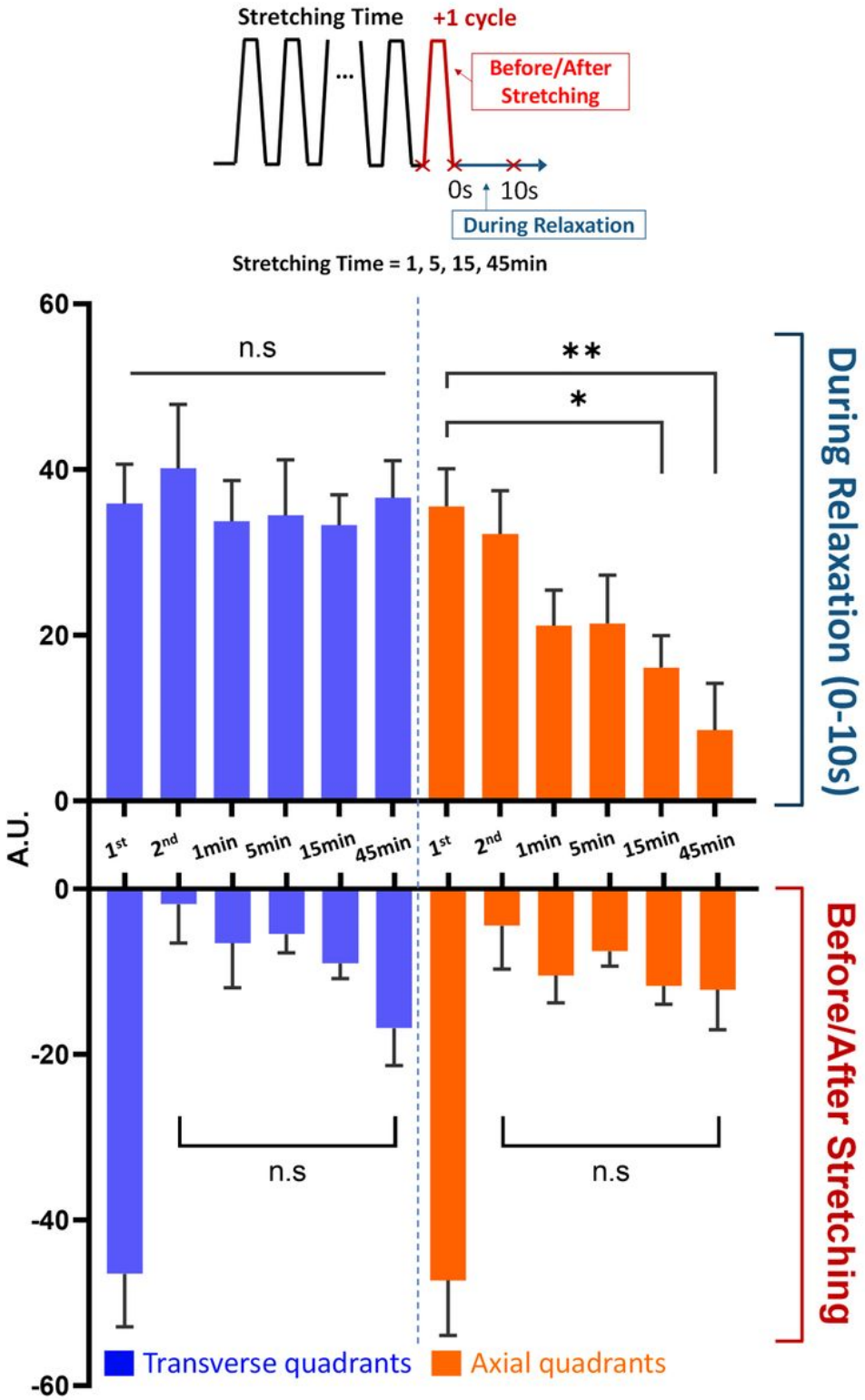

Figure 4

Differential axial and transverse responses following multiple cycles of stretching. Changes in peripheral areas are measured at the 1st cycle, 2nd cycle, and after various periods of cyclic stretching at 0.5 Hz as shown in the diagram, where the timing of image acquisition relative to the stretching cycles is indicated by red crosses. Local retractions or protrusions of different quadrants are then integrated and normalized against the total spreading area to reveal net extension (positive values) or retraction (negative values).

Net retraction takes place immediately after stretching (lower graph), while net extension takes place during subsequent 10 s of relaxation (upper graph). Moreover, net extension of axial quadrants decreases progressively with increasing cycles of stretching (top orange), while net extension of transverse quadrants remains constant (top blue). Retraction occurs similarly in all the quadrants, showing a strong response following a single cycle of stretching and a precipitous decrease with additional cycles of stretching (bottom graphs). (* $p < 0.05$; ** $p < 0.01$; n = 16- 20, Mean ± SEM.)

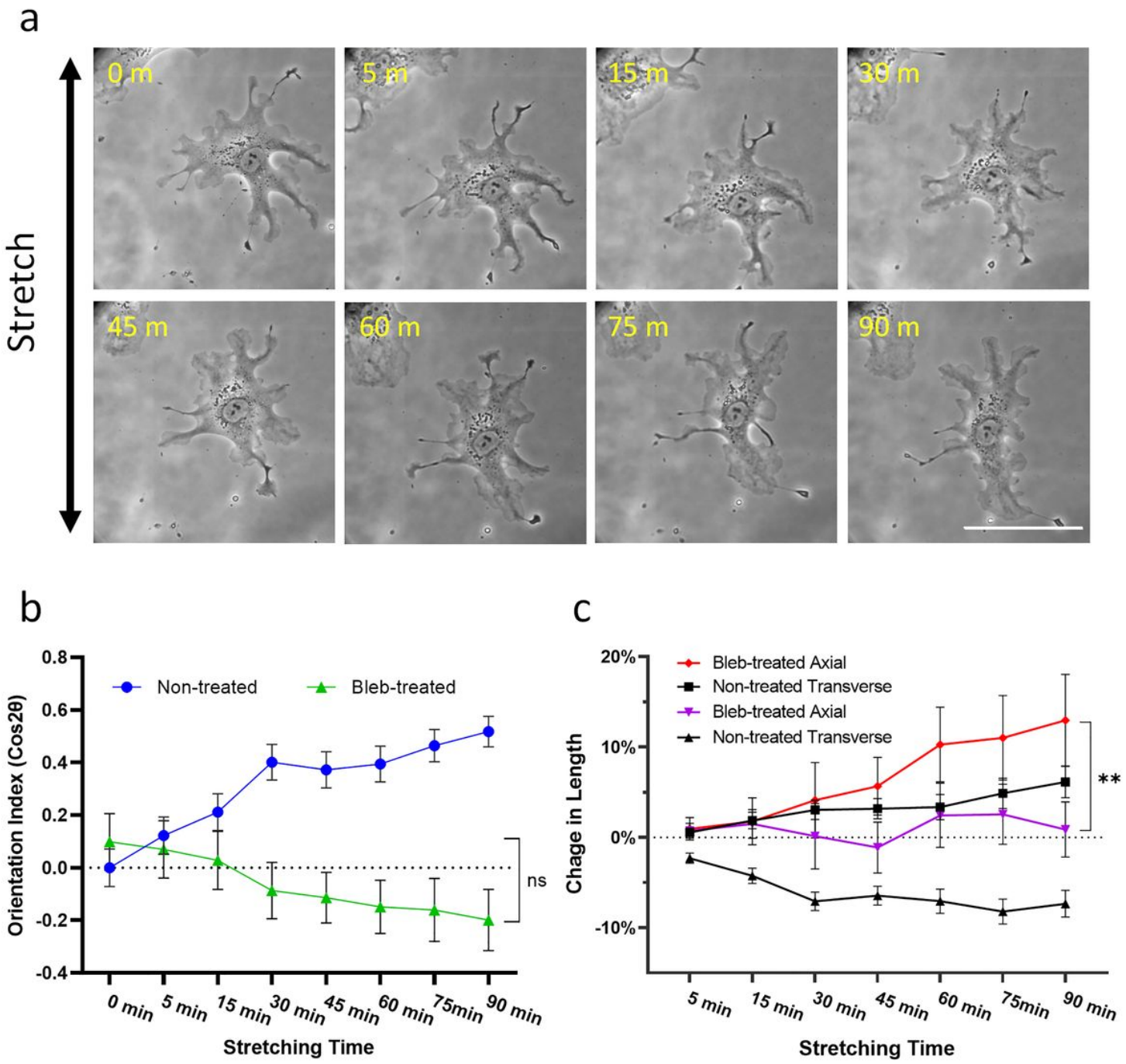

Figure 5

Effect of blebbistatin on cell reorientation and length change in response to cyclic stretching. (a) Myosin II activities are inhibited by treating cells with 50 μM blebbistatin for 30 min before applying cyclic stretching. Cells respond by elongating along axial direction (scale bar, 100 μm). (b) Unlike control cells, blebbistatin-treated cells show weakly significant axial reorientation. (c) The response to blebbistatin involves an increase in axial length and an inhibition of transverse elongation. (n.s. $p > 0.05$, ** $p < 0.01$; n = 46, Mean ± SEM.)

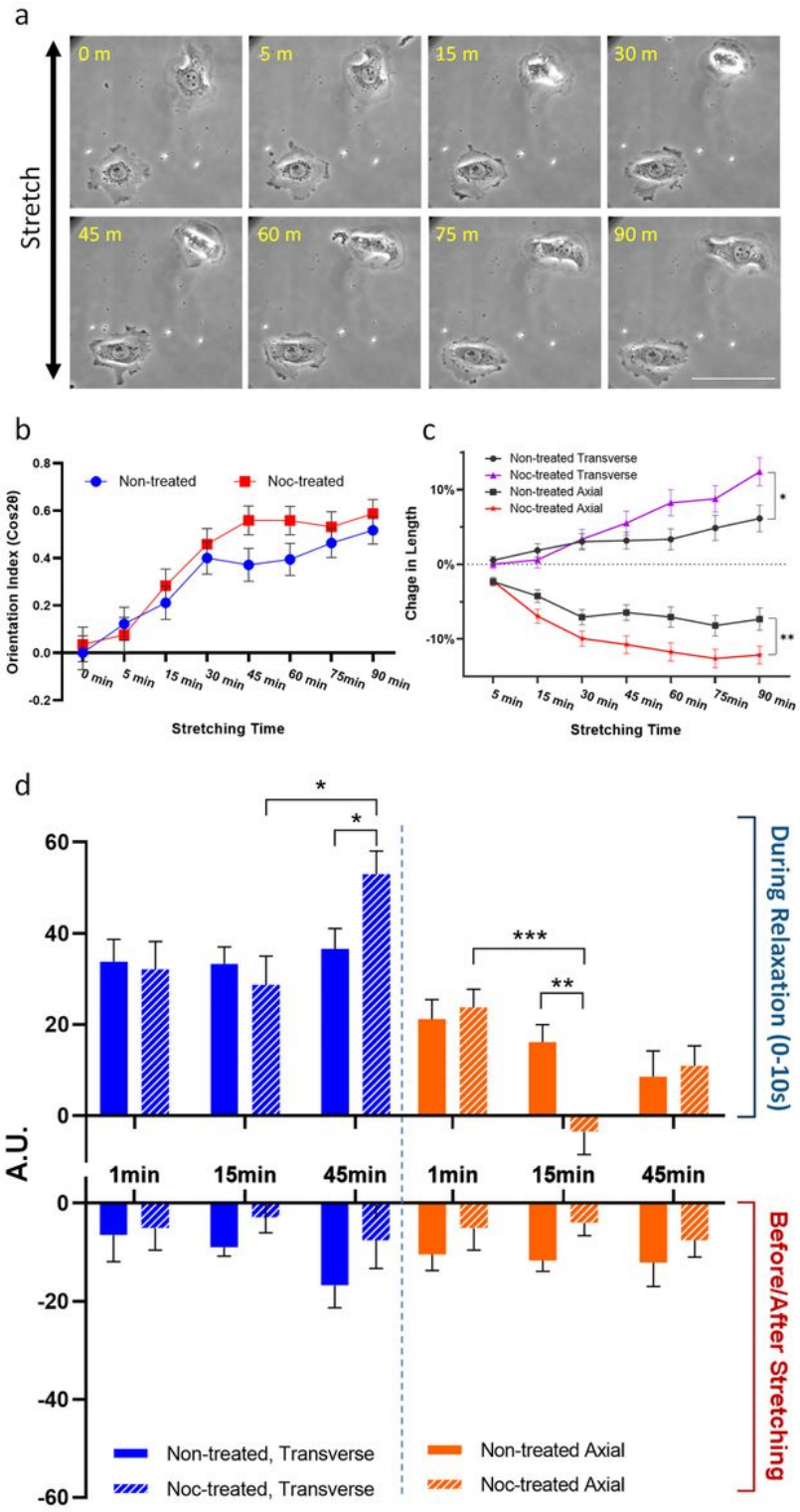

Figure 6

Effects of nocodazole on cell reorientation and length change in response to cyclic stretching. (a) Cells, treated with 5μM nocodazole for 2h before applying cyclic stretching, show more pronounced shape change and reorientation than control cells shown in Figure 2. (b and c) Comparison of control and nocodazole treated cells for reorientation and length change suggests that the effects of nocodazole take place primarily after 30min of cyclic stretching, as an increase in both transverse elongation and axial shortening (* $p < 0.05$; ** $p < 0.01$; $n = 98$, Mean ± SEM). Similar to the analysis in Fig. 4, changes of peripheral area are measured in nocodazole-treated and control cells. (d) Compared to the control (solid bars), nocodazole causes a transient inhibition of axial protrusion after 15 min of cyclic stretching (striped orange bar, upper graph), and a late stimulation of transverse protrusion at 45min (striped blue bar, upper graph). Nocodazole treated cells also show net retraction immediately after stretching (lower graph), similar to control cells. (* $p < 0.05$; ** $p < 0.01$; *** $p < 0.001$; $n = 16$ - 20, Mean ± SEM).

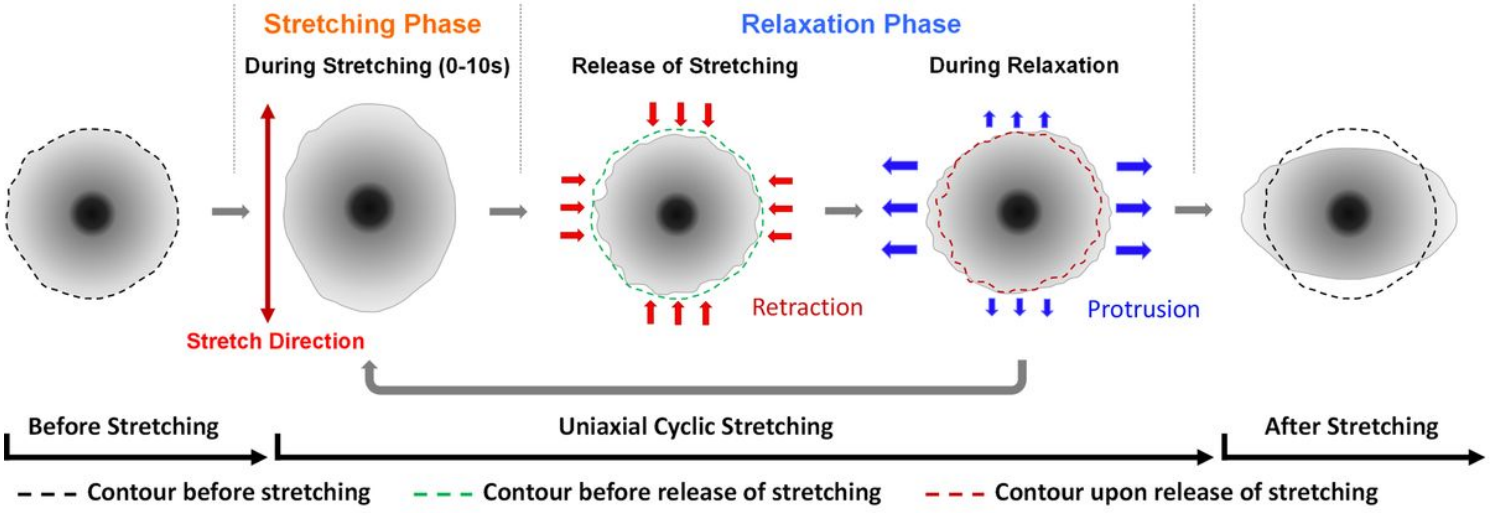

Figure 7

Summary of spatially and temporally dependent protrusion/retraction activities that lead to cell reorientation in response to uniaxial cyclic stretching. Cells (greyscale circle) retract immediately upon the release of stretching (red arrows), followed by progressive extension during the relaxation phase (blue arrows). The effects accumulate upon prolonged cyclic stretching, which leads to the change in cell shape and orientation.

Supplementary Files

This is a list of supplementary files associated with this preprint. Click to download.

- HowEpithelialCellsReorientinResponsetoCyclicStretchingSupplemetaryInformation.pdf